NeuroImage: Clinical 28 (2020) 102515

Contents lists available at ScienceDirect

NeuroImage: Clinical

journal homepage: www.elsevier.com/locate/ynicl

Transdiagnostic hippocampal damage patterns in neuroimmunological disorders

Josephine Heine [a,b], Harald Prüß [a,c], Michael Scheel [d], Alexander U. Brandt [d,e], Stefan M. Gold [f,g], Thorsten Bartsch [h], Friedemann Paul [a,d,i,j], Carsten Finke [a,i,k,*]

[a] Charité – Universitätsmedizin Berlin, Department of Neurology, Berlin, Germany
[b] Department of Psychology, Humboldt-Universität zu Berlin, Berlin, Germany
[c] German Center for Neurodegenerative Diseases (DZNE), Berlin, Germany
[d] Charité – Universitätsmedizin Berlin, NeuroCure Clinical Research Center, Berlin, Germany
[e] University of California, Department of Neurology, Irvine (CA), USA
[f] Charité – Universitätsmedizin Berlin, Department of Psychiatry and Psychotherapy and Department of Psychosomatic Medicine, Campus Benjamin Franklin, Berlin, Germany
[g] University Medical Center Hamburg-Eppendorf, Institute of Neuroimmunology and Multiple Sclerosis (INIMS), Center for Molecular Neurobiology, Hamburg, Germany
[h] University Hospital Schleswig Holstein, Department of Neurology, Kiel, Germany
[i] Charité – Universitätsmedizin Berlin, Berlin Center for Advanced Neuroimaging, Berlin, Germany
[j] Max Delbrueck Center for Molecular Medicine and Charité – Universitätsmedizin Berlin, Experimental and Clinical Research Center, Berlin, Germany
[k] Humboldt-Universität zu Berlin, Berlin School of Mind and Brain, Berlin, Germany

ARTICLE INFO

Keywords:
Hippocampal shape
Neuroinflammation
Autoimmune encephalitis
Neuromyelitis optica spectrum disorder
Multiple sclerosis
Memory disorders

ABSTRACT

Hippocampal damage and associated cognitive deficits are frequently observed in neuroimmunological disorders, but comparative analyses to identify shared hippocampal damage patterns are missing. Here, we adopted a transdiagnostic analytical approach and investigated hippocampal shape deformations and associated cognitive deficits in four neuroimmunological diseases.

We studied 120 patients (n = 30 in each group), including patients with multiple sclerosis (MS), neuromyelitis optica spectrum disorder (NMOSD), anti-NMDAR and anti-LGI1 encephalitis. A control group was matched to each patient sample from a pool of 79 healthy participants. We performed an MRI-based vertex-wise hippocampal shape analysis, extracted hippocampal volume estimates and scalar projection values as a measure of surface displacement. Cognitive testing included assessment of verbal memory and semantic fluency performance.

Our cross-sectional analyses revealed characteristic patterns of bilateral inward deformations covering up to 32% of the hippocampal surface in MS, anti-NMDAR encephalitis, and anti-LGI1 encephalitis, whereas NMOSD patients showed no deformations compared to controls. Significant inversions were noted mainly on the hippocampal head, were accompanied by volume loss, and correlated with semantic fluency scores and verbal episodic memory in autoimmune encephalitis and MS. A deformation overlap analysis across disorders revealed a convergence zone on the left anterior hippocampus that corresponds to the CA1 subfield.

This convergence zone indicates a shared downstream substrate of immune-mediated damage that appears to be particularly vulnerable to neuroinflammatory processes. Our transdiagnostic morphological view sheds light on mutual pathophysiologic pathways of cognitive deficits in neuroimmunological diseases and stimulates further research into the mechanisms of increased susceptibility of the hippocampus to autoimmunity.

1. Introduction

The hippocampus is a frequent target in many neuroimmunological diseases despite their distinct pathophysiological mechanisms. Accumulating evidence suggests a selective vulnerability of the hippocampus, and particularly its subfield CA1, to inflammatory processes (Bartsch and Wulff, 2015). Consequently, largely overlapping cognitive deficits are observed in neuroimmunological disorders, including

* Corresponding author at: Klinik für Neurologie mit Experimenteller Neurologie, Charitéplatz 1, 10117 Berlin, Germany.
E-mail address: carsten.finke@charite.de (C. Finke).

https://doi.org/10.1016/j.nicl.2020.102515
Received 7 September 2020; Received in revised form 14 November 2020; Accepted 23 November 2020
Available online 27 November 2020

impairments of episodic memory, spatial navigation and affective processing (Finke et al., 2012, 2017; Gold et al., 2014; Oertel et al., 2019). Here, we directly compared hippocampal damage and associated cognitive deficits in four distinct neuroimmunological disorders using the same imaging analysis protocol in order to explore the hypothesis of selective vulnerability and to identify shared hippocampal damage patterns.

Previous imaging studies have identified characteristic hippocampal damage patterns leading to cognitive deficits in neuroimmunological disorders. In multiple sclerosis, for example, MRI analyses revealed a hippocampal volume reduction associated with impaired verbal and visuospatial memory performance (Sicotte et al., 2008). Anti-NMDA receptor (NMDAR) encephalitis is a recently discovered autoimmune encephalitis with autoantibodies targeting the NR1 subunit of the NMDA receptor (Dalmau and Graus et al., 2018). The hippocampus contains the highest density of NMDARs and, consequently, volume loss, impaired microstructural integrity and disrupted functional connectivity of the hippocampus are characteristic imaging findings that correlate with the severity of memory impairment (Finke et al., 2016a). Autoimmune encephalitis with LGI1 antibodies manifests as limbic encephalitis with bilateral hippocampal inflammation detectable in 60–85% of patients (Finke et al., 2017; van Sonderen et al., 2016; Thompson et al., 2018). At later disease stages, almost all patients develop atrophy and impaired microstructural integrity of the hippocampus that relates to marked memory deficits (Finke et al., 2017; Kotsenas et al., 2014). In contrast, the majority of imaging studies observed no volume reduction or microstructural changes of the hippocampus in patients with neuromyelitis optica spectrum disorder (NMOSD) (Calabrese et al., 2012; Finke et al., 2016b).

However, to date, there have been no comparative approaches that characterize hippocampal damage patterns across different neuroimmunological diseases. Considering the shared cognitive symptoms, such transdiagnostic approaches can identify common downstream mechanisms that give rise to mutual clinical presentations and may therefore help to improve the pathophysiological understanding of neuropsychiatric symptoms (Husain, 2017). In addition, volumetric analyses only assess global hippocampal changes, while shape analyses can identify the exact spatial distribution of atrophy by providing discrete information about the location of pathological changes on a brain structure's surface. Indeed, shape deformations were shown to provide a sensitive marker of hippocampal pathology that can track disease progression in patients with memory disorders (Csernansky et al., 2005; Gerardin et al., 2009; Postma et al., 2020).

We therefore performed a comprehensive vertex-based shape analysis of the hippocampus in patients with four different neuroimmunological disorders, i.e. multiple sclerosis (MS), neuromyelitis optica spectrum disorder (NMOSD), anti-NMDA receptor (NMDAR) encephalitis and anti-LGI1 encephalitis. The aims of this study are to (1) describe the spatial patterns of pathological changes on the hippocampal surface, (2) provide comparative data and identify shared transdiagnostic damage patterns for these disorders, (3) and complement previous volumetric analyses by morphological assessments.

2. Materials & methods

2.1. Participants

We included one hundred twenty patients with four different neuroimmunological disorders, i.e. patients with NMDAR encephalitis (n = 30), LGI1 encephalitis (n = 30), relapsing remitting multiple sclerosis (RRMS; n = 30) and aquaporin-4 antibody positive NMOSD (n = 30). All patients were recruited from the outpatient clinics of the NeuroCure Clinical Research Center and the Department of Neurology of Charité - Universitätsmedizin Berlin between 2012 and 2017, except for eleven LGI1 encephalitis patients that were recruited at the University Hospital Schleswig-Holstein in Kiel. NMDAR encephalitis and LGI1 encephalitis patients were studied after the acute stage of the disease and were diagnosed based on the proposed criteria of characteristic clinical presentation, cerebrospinal fluid findings, neuroimaging changes and autoantibody detection (IgG NMDAR antibodies in CSF and IgG LGI1 antibodies in CSF or serum) (Graus et al., 2016). Patients with multiple sclerosis fulfilled the 2017 revised McDonald criteria and were on stable immunomodulatory therapy for at least three months, with no acute relapse for at least three months prior to enrolment and without corticosteroid therapy in the last 30 days. All NMOSD patients fulfilled the 2015 international consensus diagnostic criteria for NMOSD and were tested positive for AQP4 antibodies; no patient was MOG-antibody seropositive. Demographic and clinical descriptions of the study groups are provided in Table 1. Lesion segmentations for the characterization of MS and NMOSD patients was performed on 3D FLAIR images using the semiautomatic Lesion Segmentation Toolbox (LST) (Schmidt et al., 2012) for SPM. We created an individual control group for each clinical sample by performing a 1:1 matching (regarding age and sex) between patients and healthy control participants drawn from a pool of seventy-nine healthy volunteers.

All participants gave informed written consent. The study was approved by the Ethics Committee of Charité – Universitätsmedizin Berlin and conducted in accordance with the Declaration of Helsinki.

2.2. MRI data acquisition

A 3-dimensional, high-resolution T1-weighted sequence (Magnetization Prepared Rapid Acquisition Gradient Echo; MPRAGE, voxel size $1 \times 1 \times 1$ mm^3) and a 3D FLAIR/T2 sequence (Fluid-Attenuated Inversion Recovery; voxel size $1 \times 1 \times 1$ mm^3) were acquired for each participant on a 3T Siemens Tim Trio scanner (Siemens, Erlangen, Germany) at the Berlin Center for Advanced Neuroimaging. Eleven LGI1 encephalitis patients and matched controls were examined at the University Hospital Schleswig-Holstein in Kiel on a 3T Philips Achieva scanner using the same sequence. Study site was accounted for as a covariate in the general linear model.

2.3. Surface-based analyses and statistics

The segmentation of the left and right hippocampi was performed using FMRIB's Integrated Registration and Segmentation Tool (FIRST) as implemented in FSL (www.fmrib.ox.ac.uk). As detailed previously (Patenaude et al., 2011), the FIRST algorithm automatically segments the hippocampus based on shape models and voxel intensities. A deformable mesh model is used to create a surface mesh for each hippocampus. Each mesh is composed of a set of triangles with a fixed number of vertices, i.e. apices of adjoining triangles, for each structure. This allows for comparisons of corresponding vertices between groups. The segmentations were visually examined to confirm the accuracy of the results. For between-group comparisons, we performed separate T-tests for the left and right hippocampi using FSL Randomise with threshold-free cluster enhancement (TFCE). Contrasts were designed to test for both atrophy and growth to allow for the detection of changes in both directions. Vertex-wise T-statistics were corrected for multiple comparisons and the presented maps survived TFCE with a $q < 0.05$ FDR correction.

Next, we extracted summary statistics for the scalar projection values and volumes using the FSL-Utils toolbox. During the analysis, the surface locations of each individual's hippocampus are projected onto the cohort average surface, which reflects the mean surface position across patients and control participants. This allows a quantification of the distance between an individual's hippocampal surface and the cohort average hippocampal surface at all vertices. Scalar values represent this perpendicular distance of a vertex.

As a reference, we collected volume estimates of the hippocampi, which were corrected for intracranial volume (ICV) using the following formula: $volume_{adjusted} = volume_{raw} - \beta\ (ICV_{raw} - ICV_{mean})$; with β

Table 1
Sample characteristics. [a] Disease duration is calculated as the time span between symptom onset and time of MRI. [b] Disease severity was assessed using the modified Rankin Scale (mRS) and the Expanded Disability Status Scale (EDSS) at the study date. [c] Scoring: 0–8 no depression, 9–13 minimal depression, 14–19 mild depression, 20–28 moderate depression, 29–63 severe depression. (BDI-II: Beck Depression Inventory – Revision; RAVLT: Rey Auditory Verbal Learning Test; SRT-LTS: Selective Reminding Test – long-term storage; RWT: Regensburg Word Fluency Test; WLG: Word List Generation Test).

	NMDA	LGI1	RRMS	NMOSD
Sex				
Patients	26 f, 4 m	9 f, 21 m	18 f, 12 m	27 f, 3 m
Controls	26 f, 4 m	9 f, 21 m	18 f, 12 m	27 f, 3 m
Age				
Patients (mean (±SD))	28.0 (±7.6) yrs	65.6 (±9.1) yrs	43.3 (±6.4) yrs	45.5 (±11.1) yrs
Controls (mean (±SD))	29.0 (±8.1) yrs	62.8 (±10.3) yrs	41.8 (±8.4) yrs	44.0 (±12.5) yrs
	t(58)=−0.42, p=.68	t(58)=0.52, p=.61	t(58)=0.63, p=.53	t(58)=0.41, p=.68
Disease duration[a]	21.0 months	23.3 months	163.5 months	47.0 months
Median (range)	(2.0–82.0)	(0.2–118.2)	(17.0–346.0)	(10.0–336.0)
Disease severity[b] Median (range)	mRS 2 (0–3)	mRS 2 (0–4)	EDSS 2 (1–5)	EDSS 4 (0–6.5)
Clinical MRI				
T2 lesion count Median (range)	–	–	34 (3–126)	9 (0–68)
T2 lesion volume				
Mean (SD)	–	–	9.3 ± 7.4 ml	2.1 ± 2.3 ml
Acute phase MRI				
(No. of affected patients)	13/30 patients with abnormal MRI: Unilateral T2/FLAIR hyperintensities (temporal (5), basal ganglia (1), thalamus (1)), T2-hyperintense white matter lesions (periventricular (6), frontal/opercular (4)), mild global atrophy (1)	25/30 patients with abnormal MRI: Unilateral T2/FLAIR hyperintensities (left hippocampus (4), right hippocampus (5), right insula (1)), Bilateral T2/FLAIR hyperintensities (hippocampus (11), amygdala (5)), subcortical arteriosclerotic encephalopathy (3), periventricular leukencephalopathy (1), mild global atrophy (2)	–	–
Acute phase seizures	22/30 patients (complex-focal (2), generalized tonic-clonic (6), status epilepticus (1), unknown type (13))	FBDS: 16/30 patients Seizures: 13/30 patients (pilomotor (4), complex-focal (5), generalized tonic-clonic (4))	–	–
Therapy delay Median (range)	37 (1–1,096) days	49 (7–400) days	–	–
Memory score	RAVLT sum score	RAVLT sum score	SRT-LTS	SRT-LTS
Mean (±SD)	54.1 (±10.1)	38.0 (±12.4)	57.1 (±14.4)	56.3 (±9.2)
Norm (percentile)	40th %ile	20th %ile	52th %ile	58th %ile
Fluency score	RWT score	RWT score	WLG score	WLG score
Mean (±SD)	22.7 (±3.4)	21.5 (±4.9)	24.8 (±7.4)	26.7 (±5.6)
Norm (percentile)	35th %ile	57th %ile	31th %ile	57th %ile
BDI-II[c] Median (range)	8 (0–17)	8 (1–22)	6.5 (0–26)	11.5 (0–29)

referring to the slope of the linear regression of a participant's ICV on their raw hippocampal volume. ICV measures were determined using FSL Sienax (Smith et al., 2002). Descriptive statistics are presented with mean and standard error. Group-based analyses between patients and controls were performed using multivariate analyses of variances and receiver operating characteristics (ROC) for continuous data of the left and right hippocampus. P-values $< .05$ were considered significant. The Shapiro-Wilk test was used to assess the normality of the data.

2.4. Between-group similarity analysis

Finally, the pattern similarity of affected hippocampal surface areas was compared between diseases. To this end, the results of the normalized shape analysis were binarized for each disease group, with 1 coding a significantly affected vertex and 0 coding a non-affected surface vertex. We determined the contingency coefficient phi (Φ) for the extracted matrices using the Chi-Square test for categorical data. Φ constitutes a measure of correlation between two binary variables and allows a quantification of pattern similarity between diseases. Figures showing surface renderings were created using SurfIce (https://www.nitrc.org/projects/surfice/) and FSL FIRST3Dview.

2.5. Association with cognitive performance

Cognitive performance of patients was assessed for the purpose of correlational analyses. We assessed verbal fluency using a 1-minute semantic fluency task (category 'animals'; Regensburg Word Fluency Test (NMDA/LGI1 patients); and the identical Word List Generation subtest of the Brief Repeatable Battery of Neuropsychological Tests (BRB-N; RRMS/NMOSD patients). Verbal learning and memory were tested using two equivalent multiple-trial list-learning paradigms (German version of the Rey Auditory Verbal Learning Test (RAVLT; NMDA/LGI1 patients); Selective Reminding Test (SRT; RRMS/NMOSD patients). Depressive symptoms were assessed in all participants using the Beck Depression Inventory (BDI-II). Correlational analyses were performed using Pearson/Spearman correlation coefficients in IBM SPSS Statistics 22.

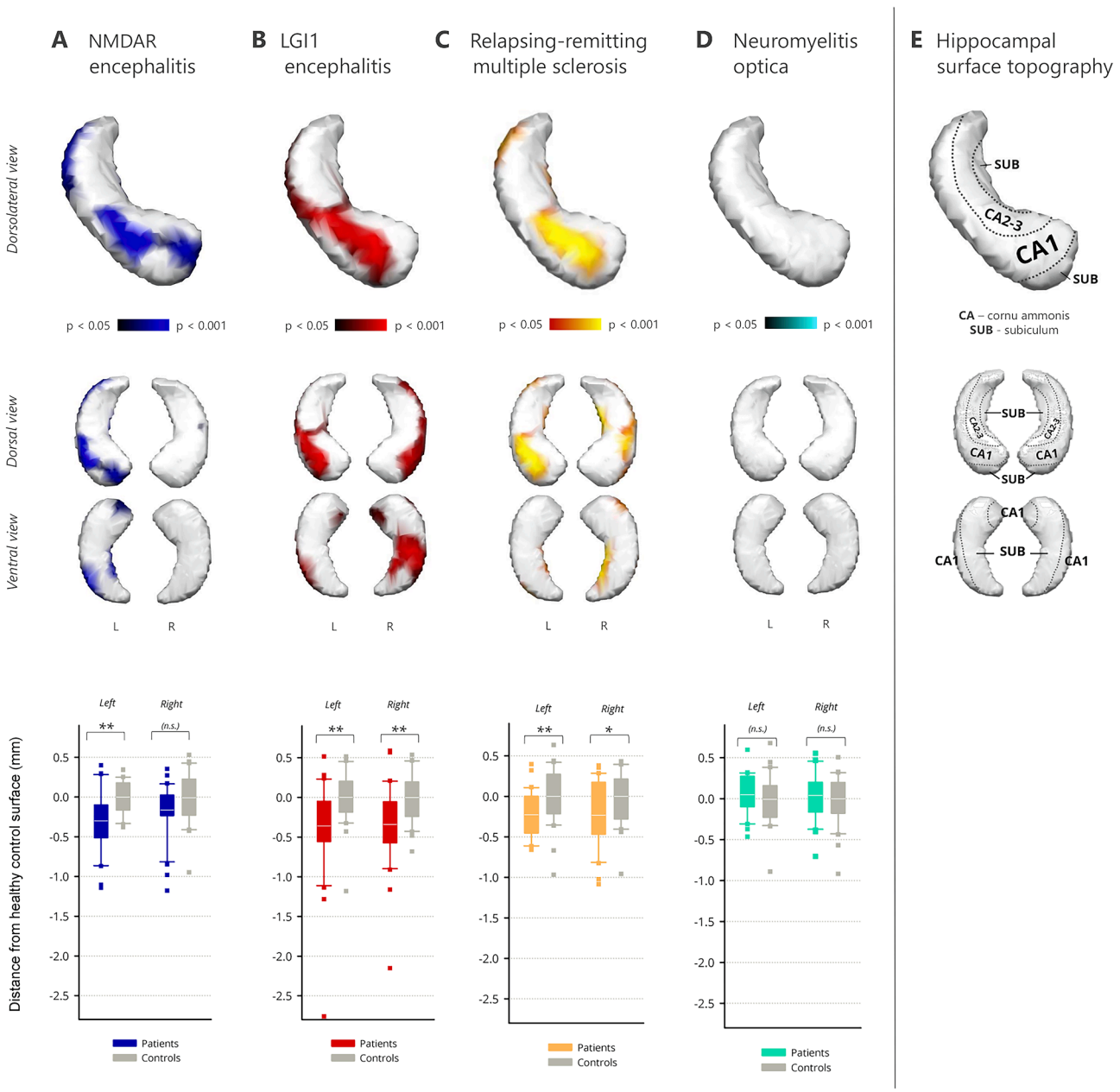

Fig. 1. Hippocampal shape deformations. Upper panels: Colored regions show significant inward deformation of the hippocampal surface ($p < .05$; multiple-comparison corrected). *Top row*: Surface deformations of the left hippocampus are shown in a dorsolateral perspective. *Bottom row*: Deformations of the left and right hippocampus are shown in ventral and dorsal view. Lower panel: Scalar projection values of the hippocampus show the average displacement of the hippocampal surface with respect to the control groups (in mm; *$p < .05$; **$p < .01$). (For interpretation of the references to colour in this figure legend, the reader is referred to the web version of this article.)

3. Results

Hippocampal deformations were observed in NMDAR encephalitis, LGI1 encephalitis and relapsing remitting multiple sclerosis (RRMS), but not in NMOSD (Fig. 1; see Fig. S1 for FDR threshold information). Volumetric results were in line with these observations (Table 2).

3.1. NMDAR encephalitis

In *NMDAR encephalitis*, an inward deformation of the surface was noted on the head of the left hippocampus (Fig. 1A). Atrophic regions extended medially and laterally along the hippocampal axis, corresponding to subfields CA1-3 and subiculum ($p < .001$). The same pattern was observed for the right hippocampus, but only two smaller clusters survived correction for multiple comparisons ($p = .034$).

We next determined the magnitude of displacement from the mean surface across the whole structure (Table 3). Surface deformations were −0.30 mm for the left hippocampus and −0.16 mm for the right hippocampus in the patient group. When compared to controls, this mean displacement of the hippocampal surface was significant for the left hippocampus ($F(1,58) = 13.88$, $p < .001$), but did not reach statistical significance for the right hippocampus ($F(1,58) = 3.71$, $p = .059$; Fig. 1A).

Correlational analyses revealed an association of the surface deformations with verbal learning performance: the stronger the inward movement of the surface cluster in the patient group, the fewer words were learned during word list learning (RAVLT sum score; $r = .335$, $p = .035$, $n = 30$). We observed no association with word fluency ($r = -.033$,

Table 2
Hippocampal volumes. Volumes were estimated using automated segmentation and corrected for intracranial volume.

		Patients (mean ± SEM)	Controls (mean ± SEM)	F	p-value	Partial η^2
NMDA	*Left*	3463.8 (±92.8) mm^3	3993.3 (±68.9) mm^3	F(1,58) = 21.0	< 0.001**	0.266
	Right	3600.3 (±87.1) mm^3	3917.7 (±89.6) mm^3	F(1,58) = 6.5	0.014*	0.100
LGI1	*Left*	3162.3 (±109.5) mm^3	3621.0 (±96.7) mm^3	F(1,58) = 9.9	0.003**	0.145
	Right	3188.5 (±105.7) mm^3	3771.9 (±88.4) mm^3	F(1,58) = 17.9	< 0.001**	0.236
RRMS	*Left*	3464.9 (±70.3) mm^3	3942.4 (±80.8) mm^3	F(1,58) = 19.9	< 0.001**	0.255
	Right	3472.1 (±103.0) mm^3	3914.3 (±80.6) mm^3	F(1,58) = 11.5	0.001**	0.166
NMOSD	*Left*	3824.8 (±70.0) mm^3	3788.3 (±84.4) mm^3	F(1,58) = 0.1	(0.740)	0.002
	Right	3835.1 (±80.1) mm^3	3802.9 (±75.5) mm^3	F(1,58) = 0.1	(0.771)	0.001

(*p < .05, **p < .01)

p = .432, n = 30), depression screening scores (r_s = −.100, p = .356, n = 16), treatment delay (r = .150, p = .237, n = 25), time since onset (r = .021, p = .455, n = 30), or functional outcome (mRS; r_s = −.120, p = .265, n = 30). In addition, both hippocampi showed a significantly reduced volume (*left:* −13.3%, F(1,58) = 20.98, p < .001; *right:* −8.1%, F(1,58) = 6.45, p = .014; Table 2).

ROC analyses revealed that surface deformations of the left hippocampus significantly differentiated between patients and controls (area under the curve (AUC) ± standard error = 0.751 ± 0.065, p = .001; Fig. 2A; Table 4). This fair to good diagnostic performance was comparable to that of volume measurements (AUC = 0.803 ± 0.058, p < .001). ROC performance for the right hippocampus was poor for both scalar displacement values (AUC = 0.636 ± 0.073, p = .070) and volumes (AUC = 0.678 ± 0.070, p = .018). Interestingly, the combination of shape and volume measures improved the classification performance for both the left (AUC = 0.823 ± 0.053, p < .001, excellent) and right hippocampus (AUC = 0.712 ± 0.067, p < .005, fair to good) as compared to any of the measures alone.

3.2. LGI1 encephalitis

LGI1 encephalitis was characterized by a significant bilateral inward movement of the hippocampal surface. Affected regions encompassed the anterior hippocampus bilaterally in the area of CA1-3 (*left,* p = .005; *right,* p = .004). Atrophy was more extensive on the right hippocampus, where it extended laterally into area CA1 towards the tail and covered almost the whole ventral posterior surface, corresponding to the subfields CA1 and subiculum (Fig. 1B).

We observed a significant surface displacement of −0.36 mm for the left (F(1,58) = 8.13, p = .006) and −0.34 mm for the right hippocampus (F(1,58) = 9.63, p = .003; Fig. 1B). Inward movement of the surface cluster correlated with decreased word fluency (r = .444, p = .017, n = 23), but not with depression screening scores (r_s = −.371, p = .117, n = 12), functional outcomes (mRS; r_s = −.146, p = .221, n = 30), or duration since onset (r = .210, p = .142, n = 28). A longer treatment delay was, however, associated with a stronger inward deformation (r = −.422, p = .020, n = 24).

While overall left hippocampal surface displacement correlated with worse verbal memory outcome (r = .348, p = .041, n = 26), no such correlation was observed in controls (RAVLT sum score; r = .032, p = .874, n = 30), suggesting that the association between surface displacement and cognition is a feature of disease pathology and not a physiological association. Volumetry revealed bilateral atrophy (*left:* −12.7%, F(1,58) = 9.86, p = .003; *right:* −15.5%, F(1,58) = 17.94, p < .001).

Surface deformations significantly differentiated between patients with LGI1 encephalitis and controls in the ROC analyses (*left:* AUC = 0.721 ± 0.066, p = .003; *right:* AUC = 0.738 ± 0.066, p = .002; Fig. 2B; Table 4). Diagnostic performance was of comparable precision in the volumetric approach (*left*: AUC = 0.723 ± 0.066, p = .003; *right*: AUC = 0.781 ± 0.059, p < .001), and improved when both measures were combined (*left:* AUC = 0.731 ± 0.065, p = .002; *right:* AUC = 0.786 ± 0.059, p < .001).

3.3. Relapsing-remitting multiple sclerosis (RRMS)

In *RRMS*, a significant bilateral inward deformation of the hippocampal surface was observed (Fig. 1C). Atrophic regions covered the anterior hippocampi in areas corresponding to the subfields CA1-3 and were more pronounced on the left side (*left,* p = .001; *right,* p = .002). Further significant clusters were noted towards the tail of the left hippocampus. On the right hippocampus, inward deformations also encompassed the whole medial surface and extended towards the tail in the subicular area.

We noted surface deformations of −0.22 mm for the left hippocampus (F(1,58) = 8.35, p = .005) and −0.24 mm for the right hippocampus (F(1,58) = 6.34, p = .015; Fig. 1C). Patients with a stronger inward movement of the affected surface area generated fewer words on the word list generation test (r = .540, p = .010, n = 18). Additionally, a stronger inward deformation was associated with a longer disease duration (r = −.583, p < .001, n = 30) and higher load of T2-hyperintense lesions (r = −0.457, p = .006, n = 30). We observed no association with verbal learning (r = .035, p = .445, n = 18), depression screening scores (r_s = 0.238, p = .103, n = 30), or functional outcomes

Table 3
Scalar projection values of the hippocampus. Total displacement values show the magnitude of the disease-related inversion of the hippocampal surface (averaged across the whole structure). Scalar values for the individual patient and control groups represent the distance to the mean surface in the analysis that is created from both groups.

		Total displace-ment	Patients (mean ± SEM)	Controls (mean ± SEM)	F	p-value	Partial η^2
NMDA	*Left*	−0.30 mm	−0.15 (±0.07) mm	0.15 (±0.04) mm	F(1,58) = 13.9	< 0.001**	0.193
	Right	−0.16 mm	−0.08 (±0.06) mm	0.08 (±0.06) mm	F(1,58) = 3.7	0.059	0.060
LGI1	*Left*	−0.36 mm	−0.18 (±0.11) mm	0.18 (±0.06) mm	F(1,58) = 8.1	0.006**	0.123
	Right	−0.34 mm	−0.17 (±0.09) mm	0.17 (±0.06) mm	F(1,58) = 9.6	0.003**	0.142
RRMS	*Left*	−0.22 mm	−0.11 (±0.05) mm	0.11 (±0.06) mm	F(1,58) = 8.4	0.005**	0.126
	Right	−0.24 mm	−0.12 (±0.07) mm	0.12 (±0.06) mm	F(1,58) = 6.3	0.015*	0.098
NMOSD	*Left*	0.06 mm	0.03 (±0.04) mm	−0.03 (±0.06) mm	F(1,58) = 0.6	(0.456)	0.010
	Right	0.04 mm	0.02 (±0.05) mm	−0.02 (±0.06) mm	F(1,58) = 0.3	(0.613)	0.004

(*p < .05, **p < .01)

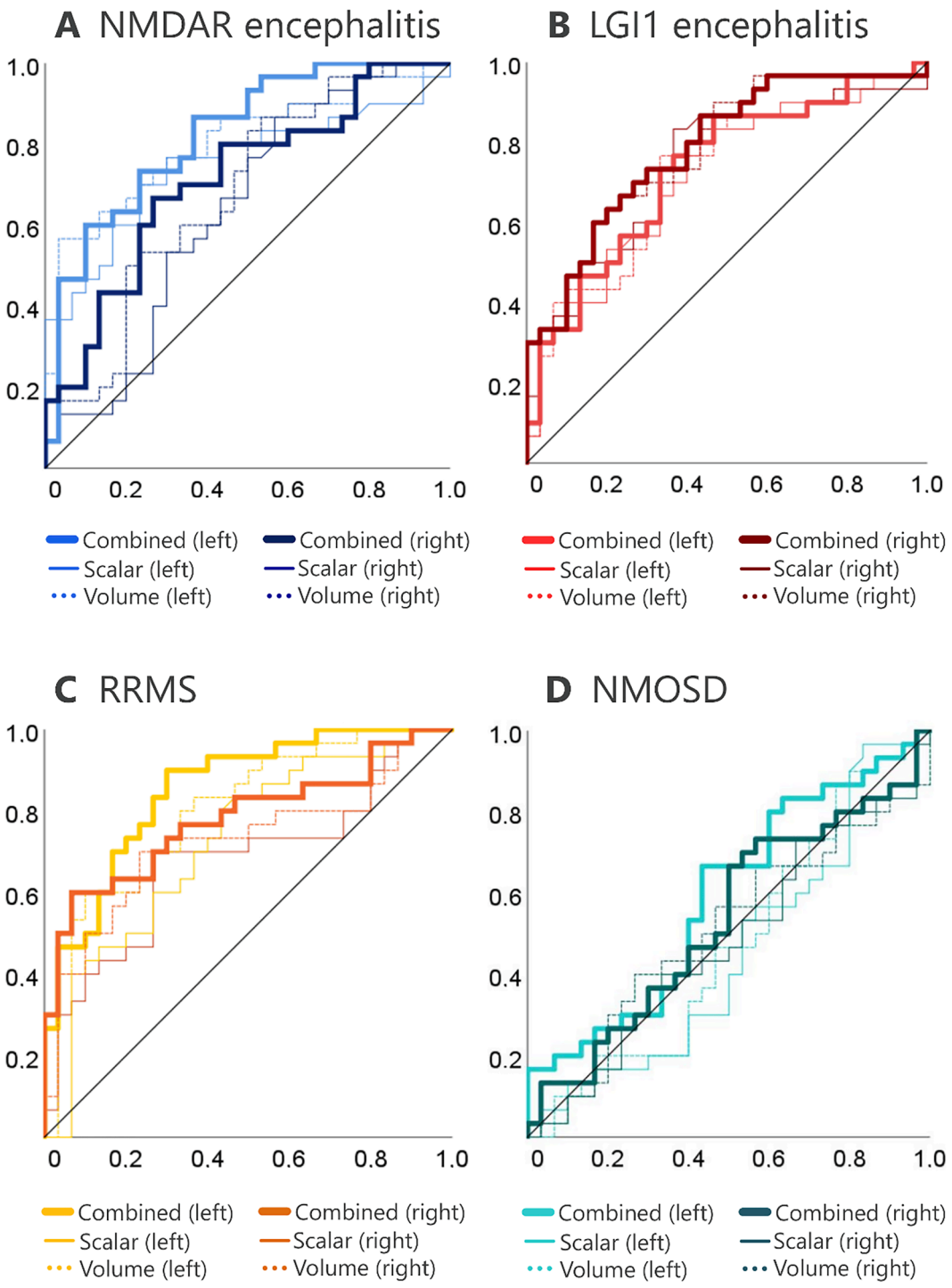

Fig. 2. Receiver operating characteristics (ROC) for hippocampal scalar values, hippocampal volumes, and their combined classification performance. 1-specificity and sensitivity of the derived displacement measure are plotted on the x and y axes. The average scalar values of the left and right hippocampi (solid lines) show comparable diagnostic performance to that of conventional volumetric measures (dotted lines). Combining shape and volume information yielded the best classification performance across all diseases.

(EDSS; $r_s = .165$, $p = .192$, $n = 30$).

Both hippocampi showed a significantly decreased volume (*left:* −12.1%, $F(1,58) = 19.9$, $p < .001$; *right:* −11.3%, $F(1,58) = 11.5$, $p = .001$). Deformations of the hippocampal surface significantly differentiated between patients with RRMS and controls (Fig. 2C; Table 4). This diagnostic performance was better for the left (AUC = 0.723 ± 0.067, $p = .003$) than for the right hippocampus (AUC = 0.678 ± 0.071, $p = .018$) and slightly inferior to that of the volumetric estimates (*left:* AUC = 0.802 ± 0.057, $p < .001$; *right:* AUC = 0.724 ± 0.068, $p = .003$). The combination of shape and volume information achieved the best classification performance (*left:* AUC = 0.853 ± 0.048, $p < .001$, excellent; *right:* AUC = 0.781 ± 0.061, $p < .001$, fair to good).

3.4. Neuromyelitis optica spectrum disorders (NMOSD)

No shape differences were observed for the left ($p = .26$) and right (p

Table 4
Receiver operating characteristics (ROC).

		Volume	Scalar	Volume + Scalar
NMDA	*Left*	0.678 (±0.070), p < .001	0.751 (±0.065), p = .001	0.823 (±0.053), p < .001
	Right	0.636 (±0.073), p = .018	0.678 (±0.070), p = .070	0.712 (±0.067), p < .005
LGI1	*Left*	0.723 (±0.066), p = .003	0.721 (±0.066), p = .003	0.731 (±0.065), p = .002
	Right	0.781 (±0.059), p < .001	0.738 (±0.066), p = .002	0.786 (±0.059), p < .001
RRMS	*Left*	0.802 (±0.057), p < .001	0.723 (±0.067), p = .003	0.853 (±0.048), p < .001
	Right	0.724 (±0.068), p = .003	0.678 (±0.071), p = .018	0.781 (±0.061), p < .001
NMOSD	*Left*	0.474 (±0.076), p = .734	0.452 (±0.076), p = .520	0.589 (±0.074), p = .237
	Right	0.502 (±0.076), p = .976	0.479 (±0.075), p = .779	0.533 (±0.076), p = .657

= .53) hippocampus in *NMOSD* patients (Fig. 1D). Mean displacement was −0.06 mm for the left and −0.04 mm for the right hippocampus, with no significant group difference (*left:* F(1,58) = 0.56, p = .46; *right:* F(1,58) = 0.26, p = .61; Fig. 1D).

Volumetric analyses showed no hippocampal atrophy (*left,* F(1,58) = 0.11, p = .740; *right,* F(1,58) = 0.09, p = .771). Accordingly, the ROC classifier performed at chance level when testing surface deformations (*left:* AUC = 0.452 ± 0.076, p = .520; *right:* AUC = 0.479 ± 0.075, p = .779), volumes (*left:* AUC = 0.474 ± 0.076, p = .734; *right:* AUC = 0.502 ± 0.076, p = .976; Fig. 2D; Table 4), and the combination of shape and volume information (*left:* AUC = 0.589 ± 0.074, p = .237; *right:* AUC = 0.533 ± 0.076, p = .657).

3.5. Overlap of surface deformations

In the next step, we quantified the surface deformation overlaps across the NMDAR encephalitis, LGI1 encephalitis and RRMS patient groups (Fig. 3). Binarized coding of the surface area revealed significant overlaps in each of the pair-wise comparisons with varying contingencies (2-sided, exact significance).

3.5.1. NMDAR encephalitis vs. RRMS

Surface deformations on the *left hippocampus* affected 32.0% of the vertices in NMDAR encephalitis and 20.8% in the multiple sclerosis group. Lesion patterns in both disorders correlated strongly (Φ = 0.440, p < .0001): 72% of the surface vertices that were affected in multiple sclerosis were also affected in NMDAR encephalitis. Vice versa, 47% of the vertices showing inversion in NMDAR encephalitis overlapped with multiple sclerosis.

On the *right hippocampus*, 26.5% of the surface vertices were significantly inverted in multiple sclerosis. Only 0.02% of the vertices were affected in NMDAR encephalitis when thresholded to a significance level of p < .05. Accordingly, the overlap was significant but with low contingency for the right side (Φ = 0.205, p < .0001; Fig. 3A) and only 7% of the vertices affected in multiple sclerosis were also deformed in NMDAR encephalitis.

3.5.2. LGI1 encephalitis vs. RRMS

Left-sided deformations covered 27.6% of the surface vertices in LGI1 encephalitis. We observed a significant overlap with moderate contingency (Φ = 0.386, p < .0001): Out of the vertices affected in LGI1 encephalitis, 46% overlapped with multiple sclerosis. Vice versa, 62% of the inverted surface vertices in multiple sclerosis were also affected in LGI1 encephalitis (Fig. 4). On the *right hippocampus*, LGI1 encephalitis affected 38.2% of the surface vertices. As observed in the previous comparison, the right-sided overlap was significant, with an albeit lower correlation (Φ = 0.260, p < .0001; Fig. 3B). Furthermore, 41% of the

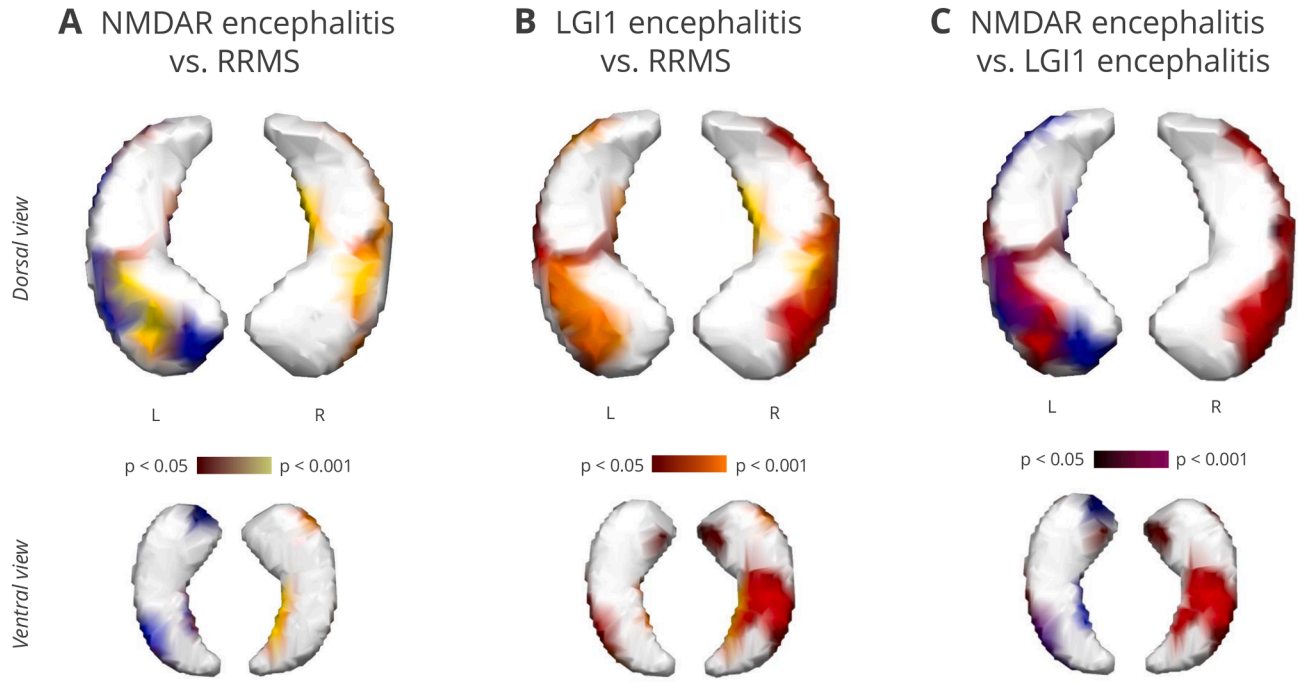

Fig. 3. Pairwise overlaps of surface deformations in ventral (upper panel) and dorsal view (lower panel). (A) Multiple sclerosis (yellow) and NMDAR encephalitis (blue) overlapped strongly on the left hippocampus (Φ = 0.440; contingency coefficient). More than 70% of the affected vertices in multiple sclerosis were also affected in NMDAR encephalitis. (B) LGI1 encephalitis (red) and multiple sclerosis (yellow) overlapped with moderate contingency on the left (Φ = 0.386) and right (Φ = 0.260) hippocampus. Surface deformations overlap around 50% on both sides. (C) Overlap of NMDAR (blue) and LGI1 encephalitis (red) was stronger for the left (Φ = 0.268) than for the right hippocampus (Φ = 0.108). Around 50% of the surface inversions overlapped. (For interpretation of the references to colour in this figure legend, the reader is referred to the web version of this article.)

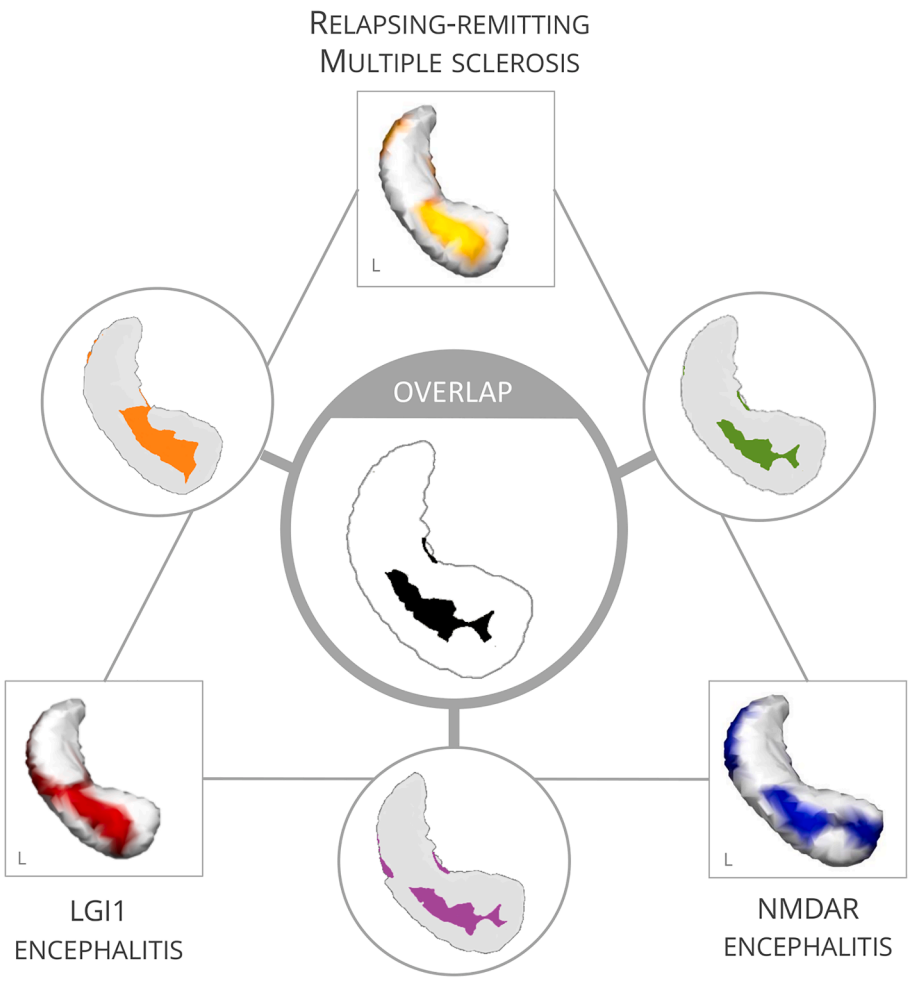

Fig. 4. Overlap analyses reveal an area of the left anterior hippocampus that is affected across diseases and sensitive to cognitive alterations.

inverted vertices in LGI1 encephalitis were also inverted in multiple sclerosis; and 59% vice versa.

3.5.3. NMDAR encephalitis vs. LGI1 encephalitis

In NMDAR and LGI1 encephalitis, affected areas overlapped significantly, but contingency was weaker than for the previous comparisons (*left*: $\Phi = 0.268$, $p < .0001$; *right*: $\Phi = 0.108$, $p < .0001$; Fig. 3C). For the *left hippocampus*, 45% of the inverted vertices in NMDAR encephalitis overlapped with LGI1 encephalitis; and 52% vice versa. Overlaps on the *right hippocampus* were negligible due to the small affected area in NMDAR encephalitis.

3.5.4. Common deformation zone in NMDAR encephalitis, LGI1 encephalitis and RRMS

Regions that were affected across NMDAR encephalitis, LGI1 encephalitis and RRMS overlapped in a convergence zone on the left anterior hippocampus corresponding to the surface area of CA1 (Fig. 4). Deformations in this overlap area correlated with cognitive performance, i.e. with verbal memory in NMDAR encephalitis ($r = .342$, $p = .032$, $n = 30$) and verbal fluency in LGI1 encephalitis ($r = .395$, $p = .031$, $n = 23$).

4. Discussion

In this study, we performed transdiagnostic hippocampal shape analyses in four neuroimmunological diseases using a unified imaging protocol. Our analysis revealed a characteristic pattern of bilateral inward deformations of the hippocampal surface in multiple sclerosis, NMDAR encephalitis and LGI1 encephalitis, but not in NMOSD. Surface deformations discriminated significantly between patients of these three disorders and controls. Higher inward deformation of the hippocampal surface predicted decreased semantic fluency in multiple sclerosis and impaired verbal memory performance in both NMDAR and LGI1 encephalitis. Analysis of deformation overlaps revealed a convergence zone in the left anterior hippocampus that corresponds to the CA1 subfield of the hippocampus and that appears to be particularly vulnerable to neuroinflammatory processes.

In NMDAR encephalitis, the most frequent subtype of autoimmune encephalitis (Dalmau and Graus, 2018), deformations were mainly observed in surface areas that correspond to the CA1-3 subfields and subiculum. Given that an inversion of the surface likely reflects volume loss of underlying tissue, it is not surprising that the location of shape deformations resembles those subfields that also showed volume loss in volumetric analyses (Finke et al., 2016a; Heine et al., 2015). Indeed, NMDAR patients had lower volumes of the subiculum as well as CA1 and CA2-3 areas. This is in line with the finding that the hippocampus, specifically CA1, contains the highest density of NMDARs in the brain (Monaghan and Cotman, 1985). Furthermore, recent studies observed functional decoupling of the hippocampus from major brain networks such as the default mode network, which was related to impaired memory performance in NMDAR encephalitis patients (Peer et al., 2017; Finke et al., 2013). The pathogenic effects of antibodies in NMDAR encephalitis are thus not only reflected in focal hippocampal damage, but also result in functional network alterations.

LGI1 encephalitis showed the most extensive shape deformations in this comparative study, covering up to 32% of the hippocampal surface area. Previous studies have shown that almost all LGI1 encephalitis

patients develop hippocampal atrophy that arises from volume loss in several subfields, including the CA1, CA2-3 areas, the dentate gyrus and subiculum (Finke et al., 2017; Miller et al., 2017). The absence of further cortical grey matter loss suggests that long-term structural damage is localized to the hippocampus (Finke et al., 2017; Miller et al., 2017), while functional connectivity alterations can involve brain-wide networks (Heine et al., 2018). Shape deformations in our study were located in the surface areas approximately corresponding to the cornu ammonis and subicular subfields. The inward movement of the bilateral surfaces correlated with impaired verbal learning and fluency, suggesting that shape alterations may represent a complementary explanation of cognitive deficits in LGI1 encephalitis.

For MS patients, our analyses show a bilateral inward deformation of the hippocampal surface associated with decreased word fluency. Beyond conventional MRI measures such as white matter lesion count or volume that do not sufficiently explain cognitive deficits, there is increasing evidence for hippocampal damage in MS (Filippi et al., 2010; Sumowski et al., 2018). Indeed, hippocampal demyelination and neuronal loss are common and can affect all hippocampal subfields (Rocca et al., 2018; Papadopoulos et al., 2009). MRI studies observed bilateral volume loss as well as impaired microstructural integrity of the hippocampus (Sicotte et al., 2008; Anderson et al., 2010; Gold et al., 2010; Planche, 2017). Additionally, recent studies showed alterations of structural and functional connectivity of the hippocampus, as well as aberrant activation during memory encoding (Rocca et al., 2018; Di Filippo et al., 2018; Hulst et al., 2012). Local pathology due to inflammatory and degenerative changes may thus interact with damage to connected white matter tracts and cortical regions (Rocca et al., 2018; Di Filippo et al., 2018) – eventually inducing widespread deficits that also affect processing speed and executive function (Paul, 2016). Hippocampal shape changes occurred bilaterally in our study and were pronounced on the left side. This cluster on the left anterior hippocampus approximately identifies as CA1 subfield but also extends to the areas of the subfields CA2-3. Importantly, previous volumetric subregion analyses revealed a similar pattern: Progressive CA1 atrophy was related to slowed processing speed, verbal and visuospatial memory deficits (Sicotte et al., 2008; Gold et al., 2010; Longoni et al., 2015). This atrophy expanded to other subfields with progression to secondary progressive multiple sclerosis (Sicotte et al., 2008). In addition, smaller CA2-3 volumes were observed in multiple sclerosis patients with depression (Gold et al., 2010). Together, these results point to a critical involvement of distinct hippocampal subregions in the pathophysiology of cognitive and affective symptoms in MS.

In contrast, we observed no shape deformations of the hippocampus in NMOSD patients. This result is in line with previous observations of normal hippocampal volumes and intact microstructural integrity in NMOSD (Finke et al., 2016b; Hyun et al., 2017). Other studies, however, found decreased hippocampal volumes in a cognitively impaired sample of Chinese patients (Liu et al., 2015), as well as in NMOSD patients with depression and anxiety symptoms (Chen et al., 2019). Whether this observation is limited to NMOSD patients with pronounced cognitive impairment or affective symptoms, or reflects differences in disease phenotypes related to ethnicity, remains an open question. Similarly, evidence for the contribution of damage to further subcortical and cortical regions to cognitive deficits in NMOSD remains inconsistent. While some studies found no cortical lesions (Calabrese et al., 2012), no cortical demyelination (Popescu et al., 2010) or subcortical volume loss (Finke et al., 2016b), others observed decreased thalamic volumes (Wang et al., 2015). In our study, we focused on AQP4 antibody-positive NMOSD patients and the apparent sparing of the hippocampus may be related to the distribution of AQP4 in periventricular and hypothalamic areas (Pittock et al., 2006). It thus remains an important open question whether hippocampal damage patterns are different in AQP4-negative NMOSD patients, and how they differ from NMOSD patients with antibodies against the myelin oligodendrocyte glycoprotein (MOG).

Shape deformations shared by NMDAR encephalitis, LGI1 encephalitis and multiple sclerosis converged on the anterolateral surface of the hippocampus, a surface area mainly covering the CA1 subfield. CA1 relays input from the CA3-DG circuitry and entorhinal cortex downstream to the subicular output areas and back to the entorhinal cortex, i.e. the hippocampal-neocortical interfaces. CA1 neurons are critically involved in memory formation and consolidation and dysfunction of these neurons leads to severe memory impairment, including input integration, mismatch and novelty detection, as well as intermediate and long-term autobiographical memory retrieval (Bartsch and Wulff, 2015; Kesner and Hunsaker, 2010). A selective vulnerability of the CA1 subfield has not only been described in limbic encephalitis (Bartsch et al., 2015) and MS (Sicotte et al., 2008), but also in other neurological disorders such as transient global amnesia, epilepsy and ischemia (Bartsch et al., 2015; Gee et al., 2006). Conceivable mechanisms for CA1 vulnerability include its high inherent degree of plasticity, local differences in antioxidant enzymes as well as calcium- and glutamate-related excitotoxicity of CA1 neurons affecting the metabolic homeostasis (Bartsch and Wulff, 2015). Interestingly, the transdiagnostic pattern of anterolateral hippocampal deformations observed in our study is also a prominent finding in Alzheimer's disease (Gerardin et al., 2009; Li et al., 2007). Mainly left-sided CA1 shape changes furthermore predicted dementia onset in healthy elderly subjects and patients with mild cognitive impairment (MCI) (Csernansky et al., 2005; Achterberg et al., 2014). In face of the overlapping nature of cognitive symptoms across neurological diseases, it has been suggested that the same ensemble of disrupted brain regions causes a clinical phenotype to arise regardless of conventional diagnostic demarcations (Husain, 2017). In line with this transdiagnostic approach, our data support the notion that damage to CA1 and its surface area is one of the main contributors to deficits of memory formation and consolidation in neuroimmunological disorders, as well as in a wide range of other neuropsychiatric diseases.

Shape changes in our samples additionally extended to surface areas that can be approximately identified as belonging to hippocampal subfields CA2 and CA3. The CA3 subregion is involved in associative memory and pattern completion (Gold and Kesner, 2005), a computational process in which entire memory representations can be recalled in response to the presentation of one of its parts. Together with the dentate gyrus, CA3 also plays a role in creating non-overlapping memory representations, a process referred to as pattern separation (Bakker et al., 2008). CA3 volume loss is observed both in autoimmune encephalitides (Finke et al., 2017, 2016a; Miller et al., 2017) and MS, particularly when depressive symptoms are present (Gold et al., 2010). Besides the autoimmune pathology, glucocorticoid receptor activation in response to disease-related behavioural stress may additionally contribute to CA2-3 (Sapolsky et al., 1990) and CA1 (Bartsch and Wulff, 2015) vulnerability.

In contrast to volumetric approaches, surface analyses provide detailed information about the location of pathological changes of the hippocampus. These analyses have been shown to discriminate between patients with neuropsychiatric disorders and controls and to reliably track disease progression. For example, morphological changes of the hippocampal surface successfully differentiated patients with MCI and patients with Alzheimer's disease (AD) from healthy controls (Gerardin et al., 2009; Li et al., 2007), with superior performance compared to volumetric measures (Gerardin et al., 2009). In schizophrenia, left–right asymmetry of hippocampal shape was observed in patients even in the absence of volume loss (Csernansky et al., 2002; Shenton et al., 2002). In line with this, we show that the combination of shape and volume information yields a better classification performance than any of the measure alone. Together with previous findings in neuropsychiatric diseases, our results suggest that shape may be a sensitive marker of – even early – damage.

Although shape analyses have made substantial contributions, some limitations need to be considered. The nature of shape analyses limits the findings of this study to the outer surface of the hippocampus. Considering the intricate hippocampal anatomy, this technique allows no assumptions about inner structures, e.g. the dentate gyrus. However,

results from our and previous studies suggest that a combination of different approaches including shape, volumetric and microstructural integrity analyses provides more detailed pathophysiological insights and yields an improved discriminatory power. In addition, despite assessing the same underlying construct and using an equivalent multiple-trial list-learning approach, minor differences in test versions used for verbal memory need to be taken into account. Future longitudinal studies may explore whether the deformations are transient or chronic, and to which extend they might serve as predictors for long-term functional outcomes.

5. Conclusion

In conclusion, we show that hippocampal shape deformations are common and highly overlapping across neuroimmunological diseases and contribute to cognitive symptoms. Our comparative approach reveals a convergence zone on the left anterolateral surface, mainly corresponding to subfield CA1 that appears to be most vulnerable to neuroinflammation - despite the distinct pathomechanisms in multiple sclerosis and autoimmune encephalitides. In this way, it improves the understanding of cognition networks in health and disease and stimulates further basic research into the mechanisms of increased susceptibility to autoimmunity of this anatomical region. This morphological view provides unique spatial information about the pattern of hippocampal lesions, transcending traditional global measures of hippocampal volume.

Funding

Funded by the Deutsche Forschungsgemeinschaft (DFG, German Research Foundation), grant numbers 327,654,276 (SFB 1315), FI 2309/1–1 (Heisenberg Program) and FI 2309/2–1; and the German Ministry of Education and Research (BMBF), grant number 01GM1908D (CONNECT-GENERATE).

Appendix A. Supplementary data

Supplementary data to this article can be found online at https://doi.org/10.1016/j.nicl.2020.102515.

References

Achterberg, H.C., et al., 2014. Hippocampal shape is predictive for the development of dementia in a normal, elderly population. Hum. Brain Mapp. 35, 2359–2371.
Anderson, V., et al., 2010. Hippocampal atrophy in relapsing-remitting and primary progressive MS: a comparative study. Mult. Scler. 16, 1083–1090.
Bakker, A., Kirwan, C. B., Miller, M. & Stark, C. E. L. Pattern Separation in the Human Hippocampal CA3 and Dentate Gyrus. Science (80-.). 319, 1640–1642 (2008).
Bartsch, T., et al., 2015. Selective neuronal vulnerability of human hippocampal CA1 neurons: lesion evolution, temporal course, and pattern of hippocampal damage in diffusion-weighted MR imaging. J. Cereb. Blood Flow Metab. 35, 1836–1845.
Bartsch, T., Wulff, P., 2015. The hippocampus in aging and disease: from plasticity to vulnerability. Neuroscience 309, 1–16.
Calabrese, M., et al., 2012. No MRI evidence of cortical lesions in neuromyelitis optica. Neurology 79, 1671–1676.
Chen, X., et al., 2019. Altered volume and microstructural integrity of hippocampus in NMOSD. Mult. Scler. Relat. Disord. 28, 132–137.
Csernansky, J.G., et al., 2002. Hippocampal deformities in schizophrenia characterized by high dimensional brain mapping. Am. J. Psychiatry 159, 2000–2006.
Csernansky, J.G., et al., 2005. Preclinical detection of Alzheimer's disease: hippocampal shape and volume predict dementia onset in the elderly. Neuroimage 25, 783–792.
Dalmau, J., Graus, F., 2018. Antibody-mediated encephalitis. N. Engl. J. Med. 378, 840–851.
Di Filippo, M., Portaccio, E., Mancini, A., Calabresi, P., 2018. Multiple sclerosis and cognition: synaptic failure and network dysfunction. Nat. Rev. Neurosci. 19, 599–609.
Filippi, M., et al., 2010. The contribution of MRI in assessing cognitive impairment in multiple sclerosis. Neurology 75, 2121–2128.
Finke, C., et al., 2012. Cognitive deficits following anti-NMDA receptor encephalitis. J. Neurol. Neurosurg. Psychiatry 83, 195–198.
Finke, C., et al., 2013. Functional and structural brain changes in anti-N-methyl-D-aspartate receptor encephalitis. Ann. Neurol. 74, 284–296.
Finke, C., et al., 2016a. Structural hippocampal damage following anti-N-methyl-D-aspartate receptor encephalitis. Biol. Psychiatry 79, 727–734.
Finke, C., et al., 2016b. Normal volumes and microstructural integrity of deep gray matter structures in AQP4+ NMOSD. Neurol. - Neuroimmunol. Neuroinflammation 3, e229.
Finke, C., et al., 2017. Evaluation of cognitive deficits and structural hippocampal damage in encephalitis with leucine-rich, glioma-inactivated 1 antibodies. JAMA Neurol. https://doi.org/10.1001/jamaneurol.2016.4226.
Gee, C.E., et al., 2006. NMDA receptors and the differential ischemic vulnerability of hippocampal neurons. Eur. J. Neurosci. 23, 2595–2603.
Gerardin, E., et al., 2009. Multidimensional classification of hippocampal shape features discriminates Alzheimer's disease and mild cognitive impairment from normal aging. Neuroimage 47, 1476–1486.
Gold, S.M., et al., 2010. Smaller cornu ammonis 2–3/dentate gyrus volumes and elevated cortisol in multiple sclerosis patients with depressive symptoms. Biol. Psychiatry 68, 553–559.
Gold, S.M., et al., 2014. Detection of altered hippocampal morphology in multiple sclerosis-associated depression using automated surface mesh modeling. Hum. Brain Mapp. 35, 30–37.
Gold, A.E., Kesner, R.P., 2005. The role of the CA3 subregion of the dorsal hippocampus in spatial pattern completion in the rat. Hippocampus 15, 808–814.
Graus, F., et al., 2016. A clinical approach to diagnosis of autoimmune encephalitis. Lancet Neurol. 15, 391–404.
Heine, J., et al., 2015. Imaging of autoimmune encephalitis - relevance for clinical practice and hippocampal function. Neuroscience 309, 68–83.
Heine, J. et al., 2018. Beyond the limbic system: disruption and functional compensation of large-scale brain networks in patients with anti-LGI1 encephalitis. J. Neurol. Neurosurg. Psychiatry DOI:10.1136/jnnp-2017-317780.
Hulst, H.E., et al., 2012. Functional adaptive changes within the hippocampal memory system of patients with multiple sclerosis. Hum. Brain Mapp. 33, 2268–2280.
Husain, M., 2017. Transdiagnostic neurology: neuropsychiatric symptoms in neurodegenerative diseases. Brain 140, 1535–1536.
Hyun, J.-W., et al., 2017. Deep gray matter atrophy in neuromyelitis optica spectrum disorder and multiple sclerosis. Eur. J. Neurol. 24, 437–445.
Kesner, R.P., Hunsaker, M.R., 2010. The temporal attributes of episodic memory. Behav. Brain Res. 215, 299–309.
Kotsenas, A.L., et al., 2014. MRI findings in autoimmune voltage-gated potassium channel complex encephalitis with seizures: one potential etiology for mesial temporal sclerosis. Am. J. Neuroradiol. 35, 84–89.
Li, S., et al., 2007. Hippocampal shape analysis of Alzheimer disease based on machine learning methods. Am. J. Neuroradiol. 28, 1339–1345.
Liu, Y., et al., 2015. Structural MRI substrates of cognitive impairment in neuromyelitis optica. Neurology 85, 1491–1499.
Longoni, G., et al., 2015. Deficits in memory and visuospatial learning correlate with regional hippocampal atrophy in MS. Brain Struct. Funct. 220, 435–444.
Miller, T.D., et al., 2017. Focal CA3 hippocampal subfield atrophy following LGI1 VGKC-complex antibody limbic encephalitis. Brain 140, 1–8.
Monaghan, D., Cotman, C., 1985. Distribution of N-methyl-D-aspartate-sensitive L-[3H] glutamate-binding sites in rat brain. J. Neurosci. 5, 2909–2919.
Oertel, F.C., Schließeit, J., Brandt, A.U., Paul, F., 2019. Cognitive impairment in neuromyelitis optica spectrum disorders: a review of clinical and neuroradiological features. Front. Neurol. 10, 34–36.
Papadopoulos, D., et al., 2009. Substantial archaeocortical atrophy and neuronal loss in multiple sclerosis. Brain Pathol. 19, 238–253.
Patenaude, B., Smith, S.M., Kennedy, D.N., Jenkinson, M., 2011. A Bayesian model of shape and appearance for subcortical brain segmentation. Neuroimage 56, 907–922.
Paul, F., 2016. Pathology and MRI: exploring cognitive impairment in MS. Acta Neurol. Scand. 134, 24–33.
Peer, M., et al., 2017. Functional connectivity of large-scale brain networks in patients with anti-NMDA receptor encephalitis: an observational study. Lancet Psychiatry 4.
Pittock, S.J., et al., 2006. Neuromyelitis optica brain lesions localized at sites of high aquaporin 4 expression. Arch. Neurol. 63, 964.
Planche, V., et al., 2017. Hippocampal microstructural damage correlates with memory impairment in clinically isolated syndrome suggestive of multiple sclerosis. Mult. Scler. J. 23, 1214–1224.
Popescu, B.F.G., et al., 2010. Absence of cortical demyelination in neuromyelitis optica. Neurology 75, 2103–2109.
Postma, T.S., et al., 2020. Hippocampal shape is associated with memory deficits in temporal lobe epilepsy. Ann. Neurol. 88, 170–182.
Rocca, M.A., et al., 2018. The hippocampus in multiple sclerosis. Lancet Neurol. 17, 918–926.
Sapolsky, R., Uno, H., Rebert, C., Finch, C., 1990. Hippocampal damage associated with prolonged glucocorticoid exposure in primates. J. Neurosci. 10, 2897–2902.
Schmidt, P., et al., 2012. An automated tool for detection of FLAIR-hyperintense white-matter lesions in Multiple Sclerosis. Neuroimage 59, 3774–3783.
Shenton, M.E., Gerig, G., McCarley, R.W., Székely, G., Kikinis, R., 2002. Amygdala-hippocampal shape differences in schizophrenia: the application of 3D shape models to volumetric MR data. Psychiatry Res. - Neuroimaging 115, 15–35.
Sicotte, N.L., et al., 2008. Regional hippocampal atrophy in multiple sclerosis. Brain 131, 1134–1141.
Smith, S.M., et al., 2002. Accurate, robust, and automated longitudinal and cross-sectional brain change analysis. Neuroimage 17, 479–489.
Sumowski, J.F., et al., 2018. Cognition in multiple sclerosis. Neurology 90, 278–288.
Thompson, J., et al., 2018. The importance of early immunotherapy in patients with faciobrachial dystonic seizures. Brain 141, 348–356.
van Sonderen, A., et al., 2016. Anti-LGI1 encephalitis: clinical syndrome and long-term follow-up. Neurology 87, 1449–1456.
Wang, Q., et al., 2015. Gray matter volume reduction is associated with cognitive impairment in neuromyelitis optica. AJNR. Am. J. Neuroradiol. 36, 1822–1829.